19. Hanson, M. M., Howarth, I. D. & Conti, P. S. The young massive stellar objects of M17. *Astrophys. J.* **489,** 698–718 (1997).
20. Nielbock, M., Chini, R., Jütte, M. & Manthey, E. High mass Class I sources in M 17. *Astron. Astrophys.* **377,** 273–284 (2001).
21. Hartmann, L. *Accretion Processes in Star Formation* (Cambridge Univ. Press, New York, 1998).
22. Wilson, C. D., Howe, J. E. & Balogh, M. L. The large-scale $J = 3 \rightarrow 2$ and $J = 2 \rightarrow 1$ CO emission from M17 and its implications for extragalactic CO observations. *Astrophys. J.* **517,** 174–187 (1999).
23. Howe, J. E. *et al.* Extended [C I] and ^{13}CO (5 → 4) emission in M17SW. *Astrophys. J.* **539,** 137–141 (2000).
24. Nakano, T., Hasegawa, T. & Norman, C. The mass of a star formed in a cloud core: Theory and its application to the Orion A cloud. *Astrophys. J.* **450,** 183–195 (1995).
25. Kobayashi, N. *et al.* IRCS: infrared camera and spectrograph for the Subaru Telescope. *Proc. SPIE* **4008,** 1056–1066 (2000).
26. Takami, H. *et al.* Performance of Subaru adaptive optics system and the scientific results. *Proc. SPIE* **4839,** 21–31 (2003).
27. Kataza, H. *et al.* COMICS: the cooled mid-infrared camera and spectrometer for the Subaru telescope. *Proc. SPIE* **4008,** 1144–1152 (2000).
28. Hogerheijde, M. R., van Dishoeck, E. F., Blake, G. A. & van Langevelde, H. J. Envelope structure on 700 AU scales and the molecular outflows of low-mass young stellar objects. *Astrophys. J.* **502,** 315–336 (1998).
29. Ohashi, N., Hayashi, M., Kawabe, R. & Ishiguro, M. The Nobeyama Millimeter Array survey of young stellar objects associated with the Taurus molecular cloud. *Astrophys. J.* **466,** 317–337 (1996).

Supplementary Information accompanies the paper on **www.nature.com/nature**.

Acknowledgements This Letter is based on data collected at the Subaru Telescope and the Nobeyama Radio Observatory, which are operated by the National Astronomical Observatory of Japan.

Competing interests statement The authors declare that they have no competing financial interests.

Correspondence and requests for materials should be addressed to S.S. (sako@ioa.s.u-tokyo.ac.jp).

Chronology of the early Solar System from chondrule-bearing calcium-aluminium-rich inclusions

Alexander N. Krot[1], **Hisayoshi Yurimoto**[2], **Ian D. Hutcheon**[3] **& Glenn J. MacPherson**[4]

[1]*Hawai'i Institute of Geophysics & Planetology, School of Ocean & Earth Science & Technology, University of Hawai'i at Manoa, Honolulu, Hawaii 96822, USA*
[2]*Department of Earth and Planetary Sciences, Tokyo Institute of Technology, Meguro, Tokyo 152-8551, Japan*
[3]*Institute of Geophysics & Planetary Physics and G.T. Seaborg Institute, Lawrence Livermore National Laboratory, Livermore, California 94451, USA*
[4]*Smithsonian Institution, Department of Mineral Sciences, NHB 119, Washington DC 20560, USA*

Chondrules and Ca-Al-rich inclusions (CAIs) are high-temperature components of meteorites that formed during transient heating events in the early Solar System. A major unresolved issue is the relative timing of CAI and chondrule formation[1–4]. From the presence of chondrule fragments in an igneous CAI, it was concluded that some chondrules formed before CAIs (ref. 5). This conclusion is contrary to the presence of relict CAIs inside chondrules[6–10], as well as to the higher abundance of ^{26}Al in CAIs[11]; both observations indicate that CAIs pre-date chondrules by 1–3 million years (Myr). Here we report that relict chondrule material in the Allende meteorite, composed of olivine and low-calcium pyroxene, occurs in the outer portions of two CAIs and is ^{16}O-poor ($\Delta^{17}O \approx -1‰$ to $-5‰$). Spinel and diopside in the CAI cores are ^{16}O-rich ($\Delta^{17}O$ up to $-20‰$), whereas diopside in their outer zones, as well as melilite and anorthite, are ^{16}O-depleted ($\Delta^{17}O = -8‰$ to $2‰$). Both chondrule-bearing CAIs are ^{26}Al-poor with initial $^{26}Al/^{27}Al$ ratios of $(4.7 \pm 1.4) \times 10^{-6}$ and $<1.2 \times 10^{-6}$. We conclude that these CAIs had chondrule material added to them during a re-melting episode ~2 Myr after formation of CAIs with the canonical $^{26}Al/^{27}Al$ ratio of 5×10^{-5}.

Mineralogical, chemical and isotopic data suggest that refractory inclusions formed in an ^{16}O-rich gaseous reservoir ($\Delta^{17}O_{SMOW} \approx -20‰$) at high ambient temperatures (near or above the condensation temperatures of forsterite; ~1,375 K at a total pressure of 10^{-4} bar), and were subsequently isolated (physically or kinetically) from reactions with the high temperature solar nebula gas[1]. (Here $\Delta^{17}O = \delta^{17}O - 0.52 \times \delta^{18}O$; $\delta^{17,18}O = [(^{17,18}O/^{16}O)_{sample}/(^{17,18}O/^{16}O)_{SMOW} - 1] \times 1{,}000$, where SMOW is Standard Mean Ocean Water.) Evaporation and condensation are believed to have been the dominant processes during formation of refractory inclusions[1]. Subsequently, some CAIs (called 'igneous') experienced extensive melting accompanied by evaporation[12]. Both igneous and non-igneous CAIs are surrounded by ^{16}O-rich multilayered rims (called 'Wark–Lovering' rims), with the outermost layers, composed of Al-diopside and forsterite, probably formed by condensation[13]. In contrast, most chondrules originated in a ^{16}O-poor ($\Delta^{17}O > -5‰$) gaseous reservoir at low (<1,000 K) ambient temperatures and higher total pressure or dust/gas ratios than CAIs[2,14–16]. Melting of pre-existing solids accompanied by evaporation-recondensation is believed to have been the dominant process during chondrule formation[2,14–16].

Most CAIs show large ^{26}Mg excesses ($^{26}Mg^*$), produced by the *in situ* decay of ^{26}Al (half-life $t_{1/2} = 0.73$ Myr), corresponding to an initial $^{26}Al/^{27}Al$ ratio, $(^{26}Al/^{27}Al)_0$, of $\sim 5 \times 10^{-5}$ (called 'canonical'), whereas most chondrules have smaller $^{26}Mg^*$ corresponding to $(^{26}Al/^{27}Al)_0$ ratios of $\leq 1.2 \times 10^{-5}$ (ref. 11 and references therein). On the basis of these observations and the assumption that ^{26}Al was uniformly distributed in the solar nebula, it is generally inferred that CAIs formed at least 1–1.5 Myr before chondrules[11]. This conclusion has recently been questioned[17] on the basis of the new lead[4] and magnesium[17] isotopic measurements. The ^{207}Pb–^{206}Pb ages of a group of Allende chondrules (4,566.7 ± 1.0 Myr)[4] cannot be distinguished from those of CV CAIs (4,567.2 ± 0.6 Myr)[2]. Bizzarro *et al.*[17] reported high precision Mg isotope analyses of micro-drilled Allende chondrules. Data for 15 chondrules show model isochrons with initial $^{26}Al/^{27}Al$ ratios ranging from $(1.4 \pm 0.5) \times 10^{-5}$ to $(5.7 \pm 0.8) \times 10^{-5}$, systematically higher than ion probe data for Allende chondrules. At face value, these results suggest that chondrule formation began contemporaneously with the formation of CAIs, and continued for at least 1.5 Myr. We note, however, that the $(^{26}Al/^{27}Al)_0$ ratios inferred from bulk Mg isotope measurements of chondrules[17] may date the time for the formation of chondrule precursor materials, not the time of chondrule melting; the latter requires Mg isotope measurements of mineral separates or individual mineral grains, which have not been completed yet. In addition, spatial heterogeneity in ^{26}Al distribution in the solar nebula cannot be ruled out. On the other hand, the relative timing of CAI and chondrule formation can be resolved by studying compound objects composed of chondrule and CAI, because both constituents of such objects were affected by the same heating episode. With one exception, all CAI-chondrule compound objects consist of relict CAIs inside chondrules, suggesting that the host chondrules formed by melting of solid precursors containing pre-existing CAIs[6–10]. The only exception is the chondrule-bearing CAI A5 from the Yamato-81020 chondrite that has been interpreted as providing evidence for chondrule formation pre-dating the formation of CAIs[5]. Here we report new observations of the mineralogy, petrography and oxygen and magnesium isotopic compositions of two chondrule-bearing CAIs (ABC and TS26) from Allende, which provide important constraints on the relative chronology of CAI and chondrule formation. Although the mineralogy and petrology of both CAIs were described previously[18,19], the presence of relict chondrule material inside them remained unnoticed.

ABC is a coarse-grained, igneous, anorthite-rich (type C) CAI fragment composed of lath-shaped anorthite (99 mole% anorthite; An_{99}) and Cr-poor Al-Ti-diopside, both poikilitically enclosing spinel grains, and interstitial, åkermanite-rich ($Åk_{74}$) melilite (Fig. 1a, b; Supplementary Table 1). A coarse fragment of forsteritic olivine (5 mole% fayalite; Fa_5) intergrown with low-Ca pyroxene (1 mole% ferrosilite, 4 mole% wollastonite; Fs_1Wo_4) occurs in the CAI portion containing Cr-rich, Al-Ti-poor diopside (Fig. 1a, c; Supplementary Table 1). The olivine-pyroxene fragment is corroded by the diopside and surrounded by a halo of high-Ca pyroxene ($Fs_{0.2–0.6}Wo_{30–40}$; Fig. 1c). Olivine and low-Ca pyroxene have ^{16}O-poor compositions; spinel and Al-Ti-diopside are moderately ^{16}O-enriched, whereas Cr-spinel, Al-Ti-poor diopside, high-Ca

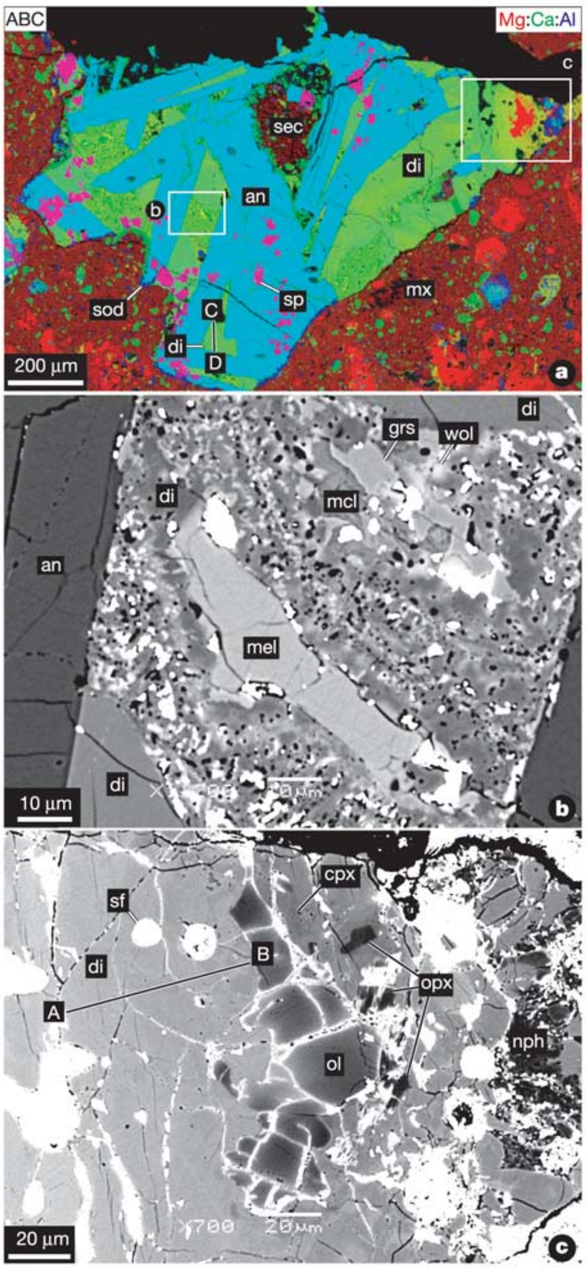

Figure 1 Type C CAI fragment ABC from Allende. **a**, Combined elemental map in Mg (red), Ca (green) and Al Kα (blue) X-rays. **b**, **c**, Backscattered electron images. Regions outlined in **a** are shown in detail in **b** and **c**. The CAI consists of coarse-grained, anorthite laths partly replaced by sodalite and nepheline, coarse-grained Al-Ti-diopside enclosing spinel grains, and interstitial material composed of fine-grained Al-diopside and melilite replaced by grossular, monticellite and wollastonite. A relict olivine-low-Ca pyroxene fragment occurs in the right portion of the CAI in the boxed area; it is surrounded by a halo of high-Ca pyroxene. A–B (in **c**) and C–D (in **a**) indicate locations of compositional profiles shown in Supplementary Fig. 1. Abbreviations: an, anorthite; cpx, high-Ca pyroxene; di, Al-Ti-diopside; grs, grossular; mcl, monticellite; mel, melilite; nph, nepheline; ol, olivine; opx, low-Ca pyroxene; sod, sodalite; sf, Fe,Ni-sulphide; sp, spinel; wol, wollastonite.

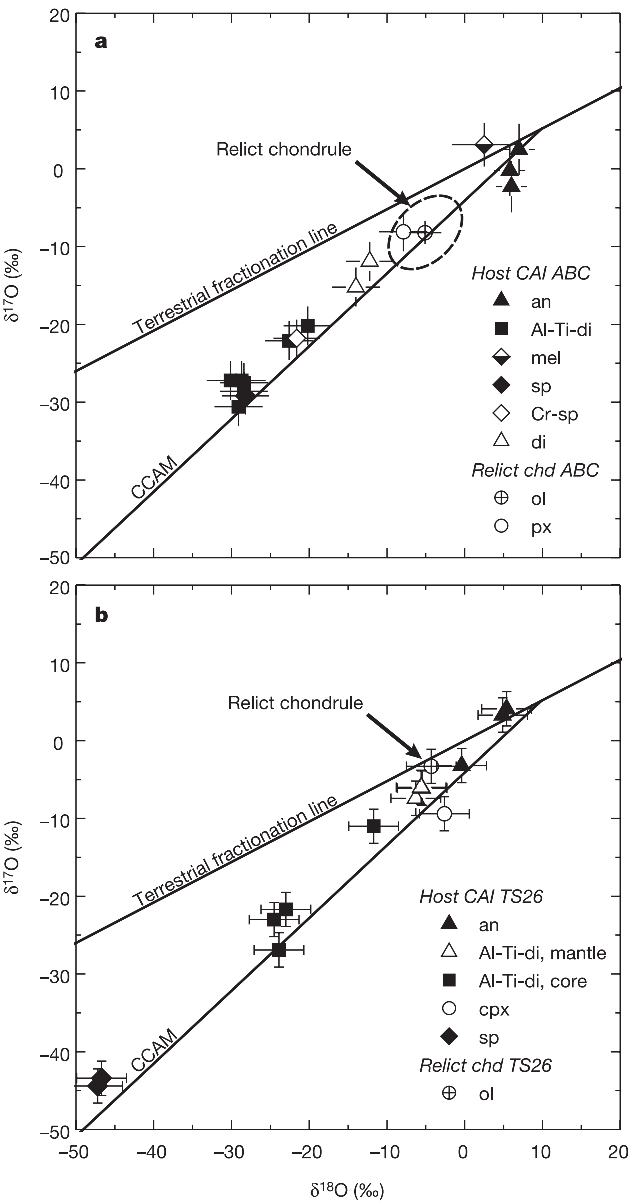

Figure 2 Oxygen isotopic compositions of chondrule-bearing CAIs from Allende. **a**, Chondrule-bearing CAI ABC. Relict olivine and low-Ca pyroxene grains have ^{16}O-poor compositions. Spinel and Al-Ti-diopside of the host CAI are ^{16}O-enriched, whereas Cr-spinel, Al-Ti-poor diopside, high-Ca pyroxene, anorthite and melilite are ^{16}O-depleted to various degrees. **b**, Chondrule-bearing CAI TS26. Relict olivine and high-Ca pyroxene halo around it have ^{16}O-poor compositions. Spinel of the CAI core is ^{16}O-rich, whereas Al-Ti-diopside and anorthite are ^{16}O-depleted to various degrees. The Al-Ti-diopside grains in the core are less ^{16}O-depleted than those in the mantle. Abbreviations: Al-Ti-di, Al-Ti-diopside; an, anorthite; chd, chondrule; di, Al-Ti-poor diopside; px, a mixture of high-Ca pyroxene (~70%) and low-Ca pyroxene (~30%); CCAM, carbonaceous chondrite anhydrous mineral line. Other abbreviations as Fig. 1. Terrestrial fractionation line and CCAM line are shown for reference. Error bars are 2σ.

pyroxene, anorthite and melilite are ^{16}O-depleted to varying degrees (Fig. 2a). The CAI shows a resolvable $^{26}Mg^*$ corresponding to a $(^{26}Al/^{27}Al)_0$ ratio of $(4.7 \pm 1.4) \times 10^{-6}$ (Fig. 3).

TS26 is an irregularly-shaped type C CAI that shows a well-defined core-mantle structure (Fig. 4a; Supplementary Fig. 2), but lacks the Wark–Lovering rim layers observed around most coarse-grained CAIs from Allende[13]. It has a coarse-grained core composed of lath-shaped anorthite (An_{99}) and sector-zoned Al-Ti-diopside, both poikilitically enclosing spinel grains, and interstitial åkermanite-rich ($Åk_{72}$) melilite. The finer-grained mantle is composed of Al-Ti-diopside, lath-shaped anorthite, and abundant coarse grains of forsteritic olivine (Fa_{8-17}) and low-Ca pyroxene (Fs_1Wo_{1-4}). The olivine and low-Ca pyroxene grains are corroded by the diopside and surrounded by haloes of high-Ca pyroxene ($Fs_{0.4-0.6}Wo_{35-42}$; Fig. 4c). Olivine and high-Ca pyroxene have ^{16}O-poor compositions; spinel is ^{16}O-rich, whereas Al-Ti-diopside and anorthite are ^{16}O-depleted to varying degrees (Fig. 2b). The coarse Al-Ti-diopside grains in the core are less ^{16}O-depleted compared to those in the finer-grained mantle. The CAI anorthite, spinel and Al-Ti-diopside show no resolvable $^{26}Mg^*$; the inferred $(^{26}Al/^{27}Al)_0$ ratio is $<1.2 \times 10^{-6}$ (Fig. 3).

The corroded appearance of olivine-pyroxene fragments in ABC and TS26 and the presence of high-Ca pyroxene haloes suggest that these grains were present inside the host CAIs during final solidification and were partly dissolved in the CAI melt. The relict origin of the olivine-pyroxene fragments is consistent with their dissolution textures and with the absence of olivine and low-Ca pyroxene in the crystallization sequence (spinel → anorthite → Al-Ti-diopside → melilite) predicted for a melt having ABC- or TS26-like bulk composition (see Supplementary Fig. 3). The coarse-grained nature of relict forsteritic olivine associated with low-Ca pyroxene and their ^{16}O-poor compositions suggest that these grains are probably fragments of ferromagnesian chondrules. Although coarse olivine grains occasionally associated with low-Ca pyroxene are also found in amoeboid olivine aggregates and in forsterite-rich accretionary rims around CAIs, these olivines and pyroxenes have characteristic ^{16}O-rich compositions[20,21].

Most coarse-grained igneous CAIs in Allende, including TS26 and ABC, show oxygen isotopic heterogeneity: spinel and Al-Ti-diopside are typically ^{16}O-rich ($\Delta^{17}O \approx -20‰$), whereas melilite and anorthite are ^{16}O-depleted ($\Delta^{17}O$ up to 5‰)[22–24]. This heterogeneity has recently been attributed to oxygen isotopic exchange between an ^{16}O-poor nebular gas and initially uniformly ^{16}O-rich CAIs during incomplete melting[23,24]. In addition, TS26 and ABC show significant ^{16}O-depletion in Al-diopside; the degree of depletion increases towards the relict chondrule fragments and the CAI peripheries. On the basis of these observations, we infer that ABC and TS26 experienced incomplete oxygen isotopic exchange and dilution with ^{16}O-poor relict chondrule materials during their

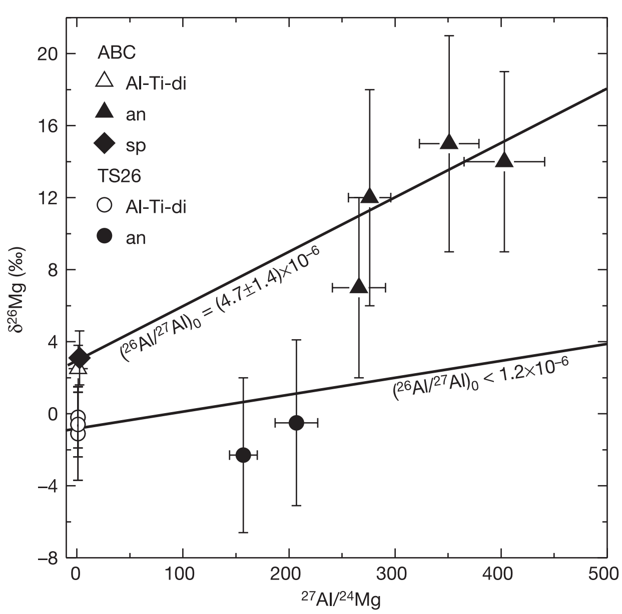

Figure 3 Al-Mg evolution diagram for the type C CAIs ABC and TS26. Error bars are 2σ.

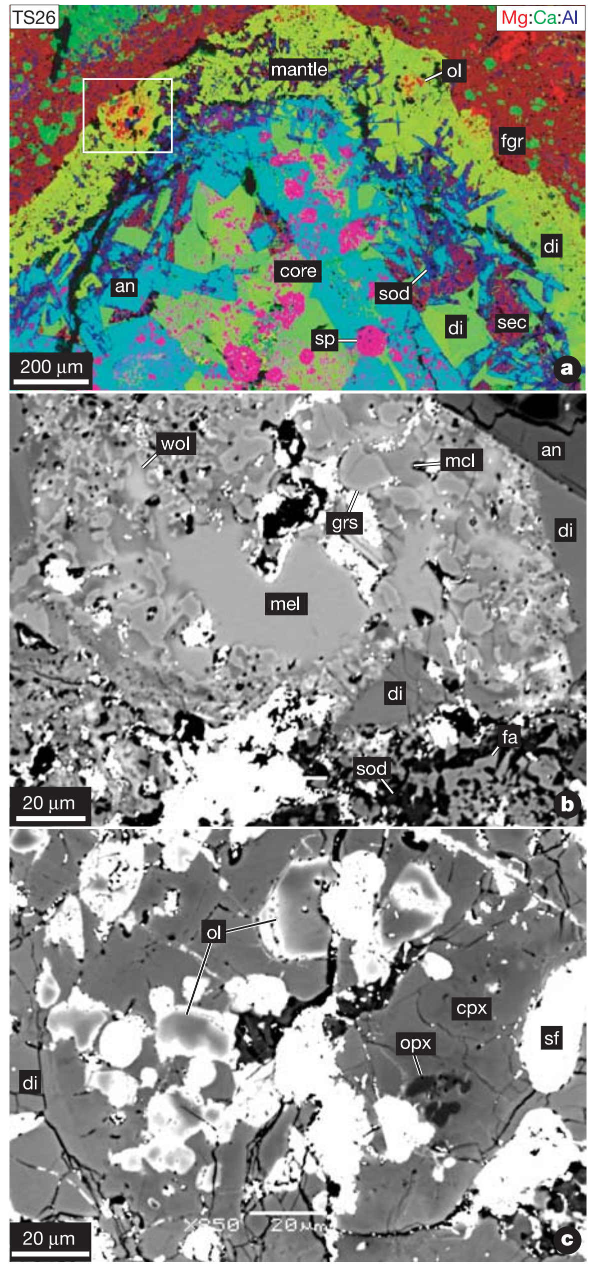

Figure 4 Type C CAI TS26 from Allende. **a**, Combined elemental map in Mg (red), Ca (green) and Al Kα (blue) X-rays. **b**, **c**, Backscattered electron images. Region outlined in **a** is shown in detail in **c**. The entire inclusion is shown in Supplementary Fig. 2. Region shown in **b** is outlined in Supplementary Fig. 2b. The CAI has a coarse-grained core composed of anorthite laths partly replaced by sodalite, Al-Ti-diopside enclosing spinel grains, and interstitial melilite replaced by grossular, monticellite, wollastonite, sodalite and ferrous olivine. The core is surrounded by a thick Al-diopside mantle containing abundant relict fragments of olivine and low-Ca pyroxene which are surrounded by haloes of high-Ca pyroxene. The mantle is separated from the core by a discontinuous layer of Fe-Ni-sulphides. The CAI is surrounded by a fine-grained rim largely composed of ferrous olivine. Abbreviations: fa, ferrous olivine; fgr, fine-grained rim. Other abbreviations as Fig. 1.

last melting in an ^{16}O-poor gas, probably in the chondrule-forming region.

The observed differences in grain size between the core and the mantle of TS26 (see Supplementary Fig. 2a) suggests that melting was incomplete and was followed by relatively fast cooling. The absence of Wark–Lovering rim layers around TS26 could also be due to the inferred melting episode. The high abundance of relict chondrule-like material in the outer portion of TS26 (see Supplementary Fig. 2b) suggests there was a high abundance of dust in the region where melting occurred, consistent with the dusty environment inferred for chondrule formation[2]. The low $(^{26}Al/^{27}Al)_0$ ratios observed in ABC and TS26 may have recorded their late-stage re-melting during incorporation of the chondrule fragments. We note, however, that because Allende experienced thermal metamorphism that may have disturbed the ^{26}Al-^{26}Mg systematics in CAIs and chondrules[25], the exact age difference between the formation of CAIs ABC and TS26 and their re-melting should be considered with caution.

The proposed multi-stage formation history of ABC and TS26 is consistent with the extended ($\sim$2 Myr) formation time of several other igneous CAI from CV chondrites inferred from a range of the $(^{26}Al/^{27}Al)_0$ ratios within a single inclusion and petrographic observations[26,27]. The late-stage melting and oxygen isotopic exchange of ABC and TS26 are also consistent with the recently proposed model for the global evolution of the oxygen isotope composition of the inner solar nebula gas from ^{16}O-rich to ^{16}O-poor with time[28,29]. The fact that many CAIs show no evidence for being affected by chondrule heating suggests that the chondrule-forming events were highly localized. □

Received 17 December 2004; accepted 11 February 2005; doi:10.1038/nature03470.

1. MacPherson, G. J. in *Treatise on Geochemistry* (eds Holland, H. D. & Turekian, K. K.) Vol. 1, *Meteorites, Comets and Planets* (ed. Davis, A. M.) 201–246 (Elsevier-Pergamon, Oxford, 2003).
2. Desch, S. J. & Connolly, H. C. A model of the thermal processing of particles in the solar nebula shocks: Application to the cooling rates of chondrules. *Meteorit. Planet. Sci.* **37,** 183–207 (2002).
3. Amelin, Y., Krot, A. N., Hutcheon, I. D. & Ulyanov, A. A. Lead isotopic ages of chondrules and calcium-aluminum-rich inclusions. *Science* **297,** 1678–1683 (2002).
4. Amelin, Y., Krot, A. N. & Twelker, E. Pb isotopic age of the CB chondrite Gujba, and the duration of the chondrule formation interval. *Geochim. Cosmochim. Acta* **68,** abstr. E958 (2004).
5. Itoh, S. & Yurimoto, H. Contemporaneous formation of chondrules and refractory inclusions in the early Solar System. *Nature* **423,** 728–731 (2003).
6. Krot, A. N. & Keil, K. Anorthite-rich chondrules in CR and CH carbonaceous chondrites: Genetic link between Ca, Al-rich inclusions and ferromagnesian chondrules. *Meteorit. Planet. Sci.* **37,** 91–111 (2002).
7. Krot, A. N., Hutcheon, I. D. & Keil, K. Anorthite-rich chondrules in the reduced CV chondrites: evidence for complex formation history and genetic links between CAIs and ferromagnesian chondrules. *Meteorit. Planet. Sci.* **37,** 155–182 (2002).
8. Krot, A. N. *et al.* Ca,Al-rich inclusions, amoeboid olivine aggregates, and Al-rich chondrules from the unique carbonaceous chondrite Acfer 094: I. Mineralogy and petrology. *Geochim. Cosmochim. Acta* **68,** 2167–2184 (2004).
9. Maruyama, S., Yurimoto, H. & Sueno, S. Oxygen isotope evidence regarding the formation of spinel-bearing chondrules. *Earth Planet. Sci. Lett.* **169,** 165–171 (1999).
10. Maruyama, S. & Yurimoto, H. Relationships among O, Mg isotopes and the petrography of two spinel-bearing chondrules. *Geochim. Cosmochim. Acta* **67,** 3943–3957 (2003).
11. McKeegan, K. D. & Davis, A. M. in *Treatise on Geochemistry* (eds Holland, H. D. & Turekian, K. K.) Vol. 1, *Meteorites, Comets and Planets* (ed. Davis, A. M.) 431–461 (Elsevier-Pergamon, Oxford, 2003).
12. Grossman, L., Ebel, D. S. & Simon, S. B. Formation of refractory inclusions by evaporation of condensate precursors. *Geochim. Cosmochim. Acta* **66,** 145–161 (2002).
13. Wark, D. A. & Lovering, J. F. Marker events in the early solar system: Evidence from rims on Ca-Al-rich inclusions in carbonaceous chondrites. *Proc. Lunar Planet. Sci. Conf.* **8,** 95–112 (1977).
14. Galy, A., Young, E. D., Ash, R. D. & O'Nions, R. K. The formation of chondrules at high gas pressures in the solar nebula. *Science* **290,** 1751–1753 (2000).
15. Alexander, C. M. O'D. & Wang, J. Iron isotopes in chondrules: Implications for the role of evaporation during chondrule formation. *Meteorit. Planet. Sci.* **36,** 419–428 (2001).
16. Scott, E. R. D. & Krot, A. N. in *Treatise on Geochemistry* (eds Holland, H. D. & Turekian, K. K.) Vol. 1, *Meteorites, Comets and Planets* (ed. Davis, A. M.) 143–200 (Elsevier-Pergamon, Oxford, 2003).
17. Bizzarro, M., Baker, J. A. & Haack, H. Mg isotope evidence for contemporaneous formation of chondrules and refractory inclusions. *Nature* **431,** 275–278 (2004).
18. MacDougall, J. D., Kerridge, J. F. & Phinney, D. Refractory ABC. *Lunar Planet. Sci.* **12,** 643–645 (1981).
19. Wark, D. A. Plagioclase-rich inclusions in carbonaceous chondrite meteorites: Liquid condensates? *Geochim. Cosmochim. Acta* **51,** 221–242 (1987).
20. Krot, A. N., McKeegan, K. D., Leshin, L. A., MacPherson, G. J. & Scott, E. R. D. Existence of an ^{16}O-rich gaseous reservoir in the solar nebula. *Science* **295,** 1051–1054 (2002).
21. Krot, A. N., Fagan, T. J., Yurimoto, H. & Petaev, M. I. Origin of low-Ca pyroxene in amoeboid olivine aggregates: Evidence from oxygen isotopic compositions. *Geochim. Cosmochim. Acta* (in the press).
22. McKeegan, K. D. & Leshin, L. A. in *Stable Isotope Geochemistry* (eds Valley, J. W. & Cole, D. R.) 279–378 (Reviews in Mineralogy & Geochemistry, Vol. 43, Mineralogical Society of America, Washington DC, 2001).
23. Yurimoto, H., Ito, M. & Nagasawa, H. Oxygen isotope exchange between refractory inclusion in Allende and solar nebula gas. *Science* **282,** 1874–1877 (1998).
24. Nagashima, K., Yoshitake, M. & Yurimoto, H. in *Workshop on "Chondrites and the Protoplanetary Disk"* 153–154 (University of Hawaii at Manoa, 2004); available at ⟨http://www.lpi.usra.edu/meetings/chondrites2004/pdf/9072.pdf⟩.
25. Yurimoto, H., Koike, O., Nagahara, H., Morioka, M. & Nagasawa, H. Heterogeneous distribution of Mg isotopes in anorthite single crystal from Type B CAIs in Allende meteorite. *Lunar Planet. Sci.* **31,** 1593 (2000).
26. MacPherson, G. J. & Davis, A. M. A petrologic and ion microprobe study of a Vigarano Type B refractory inclusion: Evolution by multiple stages of alteration and melting. *Geochim. Cosmochim. Acta* **57,** 231–243 (1989).
27. Hsu, W., Wasserburg, G. J. & Huss, G. R. High time resolution by use of the ^{26}Al chronometer in the multistage formation of a CAI. *Earth Planet. Sci. Lett.* **182,** 15–29 (2000).
28. Yurimoto, H. & Kuramoto, K. Molecular cloud origin for the oxygen isotope heterogeneity in the solar system. *Science* **305,** 1763–1766 (2004).
29. Krot, A. N. *et al.* Evolution of oxygen isotopic composition in the inner solar nebula *Astrophys. J.* (in the press).

Supplementary Information accompanies the paper on **www.nature.com/nature**.

Acknowledgements Financial support for this project was provided by NASA (A.N.K., I.D.H., G.J.M.) and Monkasho (H.Y.). We thank R. H. Hewins for comments and suggestions.

Competing interests statement The authors declare that they have no competing financial interests.

Correspondence and requests for materials should be addressed to A.N.K. (sasha@higp.hawaii.edu).

Controlled multiple quantum coherences of nuclear spins in a nanometre-scale device

Go Yusa[1], Koji Muraki[1], Kei Takashina[1], Katsushi Hashimoto[2]* & Yoshiro Hirayama[1,2]

[1]*NTT Basic Research Laboratories, NTT Corporation, 3-1 Morinosato-Wakamiya, Atsugi 243-0198, Japan*
[2]*SORST Program, Japan Science and Technology Agency (JST), 4-1-8 Honmachi, Kawaguchi, Saitama 331-0012, Japan*

* Present address: Institute of Applied Physics, Hamburg University, Jungiusstraβe 11, D-20355 Hamburg, Germany

The analytical technique of nuclear magnetic resonance (NMR[1,2]) is based on coherent quantum mechanical superposition of nuclear spin states. Recently, NMR has received considerable renewed interest in the context of quantum computation and information processing[3–11], which require controlled coherent qubit operations. However, standard NMR is not suitable for the implementation of realistic scalable devices, which would require all-electrical control and the means to detect microscopic quantities of coherent nuclear spins. Here we present a self-contained NMR semiconductor device that can control nuclear spins in a nanometre-scale region. Our approach enables the direct detection of (otherwise invisible) multiple quantum coherences between levels separated by more than one quantum of spin angular momentum. This microscopic high sensitivity NMR technique is especially suitable for probing materials whose nuclei contain multiple spin levels, and may form the basis of a versatile multiple qubit device.

Nuclei often possess total spin I greater than a half. Under static magnetic field B_0, therefore, $2I+1$ states $|m\rangle$ equally spaced in energy by the Zeeman energy $\hbar\omega_0$ are formed according to the Zeeman effect (Fig. 1e). Here, $\hbar$ is the reduced Planck's constant such that ω_0 would be the resonant angular frequency of NMR between any pair of adjacent states. After appropriate polarization,